Nanoscale Advances

ROYAL SOCIETY OF CHEMISTRY

PAPER

View Article Online
View Journal | View Issue

Cite this: *Nanoscale Adv.*, 2022, **4**, 5355

Sugar-decorated carbon dots: a novel tool for targeting immunomodulatory receptors†

Oren Cooper,[a] Mario Waespy,[b] Dechao Chen,[c] Sørge Kelm,[b] Qin Li,[cd] Thomas Haselhorst*[a] and Joe Tiralongo*[a]

Interactions between sialic acid (Sia) and sialic acid-binding immunoglobulin-like lectins (siglecs) regulate the immune system, with aberrations contributing to pathologies such as autoimmunity, infectious disease and cancer. Over the last decade, several multivalent Sia ligands have been synthesized to modulate the Sia-binding affinity of proteins/lectins. Here, we report a novel class of multivalent siglec probes through the decoration of α(2,6)-sialyllactose ligands on inherently fluorescent carbon dots (CD). We show that the preference of α(2,3)-linked Sia for siglec-1 can be altered by increasing the multivalence of Sia ligands present on the CD, and that a locally high glycan concentration can have a direct effect on linkage specificity. Additionally, micromolar (IC_{50} ~ 70 μM) interaction of α(2,6)-sialyllactose-CD (6-CD) with siglec-2 (CD22) revealed it was capable of generating a significant cytotoxic effect on Burkitt's Lymphoma (BL) Daudi B cells. This phenonomen was attributed to 6-CD's ability to form *trans* interactions with CD22 on masked BL Daudi cells as a direct result of clustering of the Sia moiety on the CD surface. Overall, our glycoengineered carbon dots represent a novel high affinity molecular probe with multiple applications in sialoglycoscience and medicine.

Received 10th June 2022
Accepted 14th October 2022

DOI: 10.1039/d2na00364c

rsc.li/nanoscale-advances

Introduction

The regulatory functions of sialic acid binding immunoglobulin-like lectins (siglecs) represent promising therapeutic strategies for a wide range of immunological disorders and cancer (immunoglyco-therapy).[1,2] Siglecs are type I membrane proteins displaying an amino terminal V-set immunoglobulin domain that binds sialic acids (Sia) attached to terminal regions of cell surface glycoconjugates. Of these, siglec-2 (CD22) is of pivotal importance in B cell activation and as such an attractive target for therapies of autoimmune diseases and B cell derived non-Hodgkin's lymphoma. CD22 is a B cell-specific transmembrane protein of the Ig superfamily with seven Ig-like domains. Previous studies in mice, have demonstrated that CD22 has two distinct functions, firstly its association with the B cell receptors (BCR) followed by inhibition of the BCR signal (see ESI Fig. S1†).[3–6] CD22 has known lectin properties and binds with high preference to α(2,6)-linked Sia in either *cis* configuration on the B cell surface or in *trans* configuration on the surface of other cells, soluble glycoproteins and cell-associated antigens.[7–9] As periphery B cells usually display high levels of α(2,6)-linked Sia on the cell surface, CD22 will bind them with high affinity.[10,11]

The majority of research targeting siglecs has been directed at antigen therapies,[12–14] however as an alternative, multivalent sialoglycan ligands have emerged as promising tools targeting siglecs.[15] Kiessling and co-workers for example constructed a copolymer that composed the BCR-binding epitope and the CD22-specific ligand. The authors found that *trans*-interactions between CD22 and Sia glycans are regulated by the activation of BCR. These copolymers enabled the simultaneous targeting of BCR and CD22 receptors, induced *trans*-interactions in the CD22 signaling, activating several pathways.[16]

The natural Sia ligand for CD22 typically occurs on the same cell (in *cis*) and/or on adjacent cells (in *trans*). *cis* ligands mask the binding of sialoside ligands and are thought to regulate the activity of CD22 as modulators of cell signalling.[17] This has made it challenging to design targeted siglec monovalent sialosides.[18–24] To address this, multivalent ligands of sufficient avidity have been shown to be able to compete with *cis* ligands, demonstrating a dynamic equilibrium of *cis* and *trans* ligand probes.[25,26] The use of sialosides on nanoparticles as multivalent Sia ligands is limited.[27–32] To date, the most suitable architectures for multivalent presentation of CD22 ligands are liposomes.[33–37] Chen and co-workers have shown that doxorubicin loaded liposomes

[a]*Institute for Glycomics, Gold Coast Campus, Griffith University Queensland, 4222 Australia. E-mail: t.haselhorst@griffith.edu.au; j.tiralongo@griffith.edu.au*
[b]*Centre for Biomolecular Interactions Bremen, Department of Biology and Chemistry, University of Bremen, 28334 Bremen, Germany*
[c]*School of Engineering and Built Environment, Nathan Campus, Griffith University, QLD 4111, Australia*
[d]*Queensland Micro- and Nanotechnology Centre, Australia, Nathan Campus, Griffith University, QLD 4111, Australia*

† Electronic supplementary information (ESI) available. See DOI: https://doi.org/10.1039/d2na00364c

bearing ligands for CD22 are effective drug delivery vehicles for depletion of B cells *in vivo*.[35] These studies highlight the importance of multivalent presentation of the Sia ligand for targeting of CD22-expressing cells.

Recent advances in glyco-nanotechnology has allowed the development of novel multivalent scaffolds that possess, at the nanoscale, inherent photonic,[38] fluorescent,[39] electronic,[40] and magnetic[41] properties to explore carbohydrate–lectin interactions in an unparalleled manner. Of these, quantum dots (QDs)[42–45] and carbon dots (CDs)[46,47] have been explored as suitable tools for cell targeting. QDs and CDs are zero-dimensional nano-architectures that are intrinsically fluorescent,[48] which due to their high surface/volume ratios and abundant surface functional groups are capable of enhancing avidity, allowing researchers to exploit multivalent interactions. These platforms thus represent an ideal route for glycan-based cell targeting, for example as drug delivery systems or imaging agents and can be used as a diagnostic platform and biosensing tool making them highly promising theranostic devices.

In our previous work, we explored the use of CDs as multivalent scaffold for lactose.[47] Here, self-assembled glycan monolayers (SAGM) were generated by functionalizing lactose with an epoxy linker, (3-glycidyloxypropyl)trimethoxysilane (GOPTS). Subsequent passivation of these SAGM to CDs provided us with a multivalent glycan coat to explore the effect lactose has on intracellular localization of CDs in cultured cells. Given our success with lactose, we have extended our approach to other glycan classes. To this end, we have engineered multivalent CDs using our SAGM method to target CD22 for BCR inhibition (see Fig. 1).

Experimental procedures

General procedures

All chemicals were purchased from Sigma-Aldrich and used without further purification. α2,3-Sialyllactose (2,3-SL) and α2,6-sialyllactose (2,6-SL) were purchased from Elicityl (France). Lactose (anhydrous) was purchased from Sigma-Aldrich. Glassware and syringes used for reactions requiring anhydrous solvents were dried in an oven (100 °C) for at least 2 h and allowed to cool in a desiccator. Liquid reagents, solutions or solvents were added *via* syringe through a rubber septum. Reactions were monitored through thin-layer chromatography (EtOAc/MeOH/H_2O (3 : 2 : 0.2)) on TLC silica gel 60 F_{254} with UV light (365 nm) detection and by charring with 7% sulfuric acid in ethanol. Products were concentrated *in vacuo* using both a Büchi rotary evaporator R-114 (bath temperature set to 40 °C at a pressure of 15 mmHg) and a high vacuum line at room temperature. Water soluble compounds were freeze dried on a LDC 1 M Martin Christ Alpha 1–4. ^{1}H NMR and ^{13}C NMR spectra were measured in the solvent stated in a 400 MHz NMR spectrometer (Bruker) for the outlined reaction steps. The photoluminescence spectra of excitation and emission and absorption spectra of sample were recorded using Duetta (Horiba) fluorescence and absorbance spectrophotometer. ^{1}H NMR spectra were obtained using a Bruker 400 MHz spectrometer. TEM was performed on a JEOL-2100 high-resolution transmission electron microscope with a voltage of 200 kV. FTIR spectral analysis was performed using a Bruker Alpha Fourier Transform Infra-Red spectrometer. Dynamic light scattering (DLS) and ζ analysis were carried out using a Nano ZS

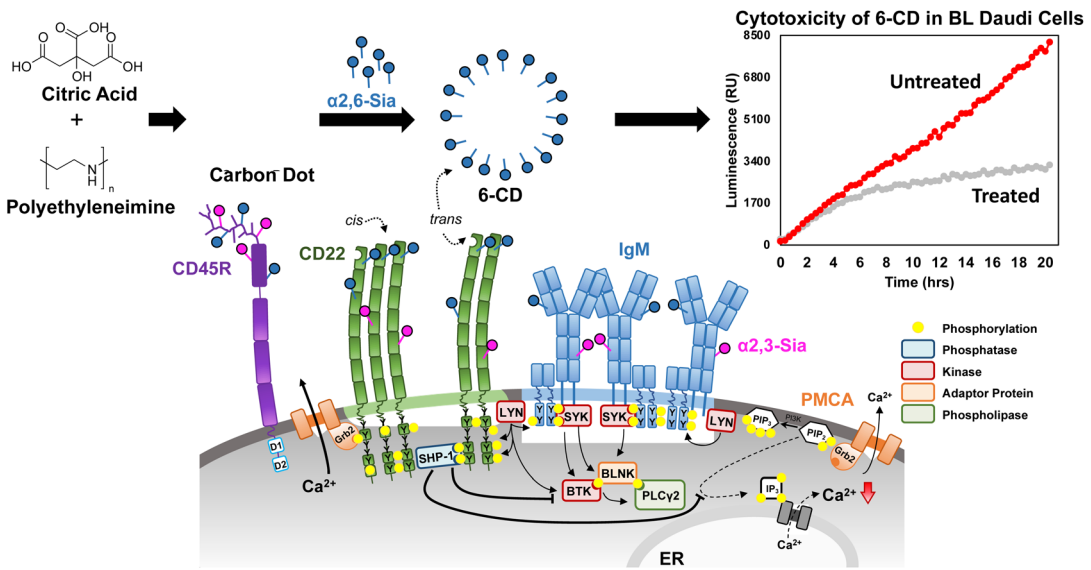

Fig. 1 Targeting CD22 in Burkitts Lymphoma (BL) Daudi cells. The B cell receptor (BCR) is closed in resting B cells and CD22 forms homo-oligomers through *cis*-interactions with α(2,6)-linked Sia. For signal inhibition, CD22 needs to be recruited to the BCR which can occur through binding ligands of other cells or as illustrated here with carbon dots, *via trans*-interactions. Here, the proximity of CD22 to BCR leads to phosphorylation of the ITIMs of CD22 by LYN. Subsequent signaling cascades through SHP-1 dephosphorylation inhibit further Ca^{2+} release and negatively regulate the BCR signal. In our work, we demonstrate interaction of α(2,6)-sialyllactose-CD (6-CD) is capable of interacting with CD22 in *trans* leading to a significant cytotoxic effect. A more detailed insight into the regulation of the BCR is given in the ESI Fig. S1.†

(Malvern Instruments). 384- and 96-well plate experiments were measured using an Infinite M200 Pro Multimodal Plate reader (Tecan) in various configurations (absorbance, fluorescence or luminescence) depending on the indicated readout.

Carbon dot synthesis and glycan functionalization

Carbon dot synthesis and characterizations. The hydrothermal synthesis of CDs followed our previously established procedure.[49] A typical synthesis required dissolving of 0.5 g of citric acid and 10 mL of polyethyleneimine (PEI) (MW ~ 800) in 5 mL of distilled water. The mixture was sonicated for 1 min to form a transparent solution. The solution **1** was then transferred in a 30 mL Teflon-lined stainless-steel autoclave and treated at 180 °C in an oven for 6 h (see Scheme 1). After reaction, the mixture was then cooled to room temperature and appeared as a light-yellow clear solution. The suspension was filtered through a Millipore syringe filters with the pore size of 0.22 μm followed by dialysis **2** (1 K MWCO, Spectrum Inc.) against deionised water to remove the unreacted molecules. Finally, the particles >1 kDA were lyophilized overnight and resuspended in anhydrous methanol. Hereafter this PEI functionalized CD is referred to as uCD and serves as the principal scaffold for subsequent glyco-coating using SAGM. As the glycocoat is absent on uCD we can considered it "uncoated".

Glycan conjugation to carbon dot. In separate round bottom flasks, 100 mg of lactose, 2,6-SL and 2,3-SL was aminated as described.[50] Briefly, glycans were dissolved with 5-fold excess (w/w) ammonium carbonate in ammonium hydroxide and left sealed and stirring at 50 °C. After 3 days, the seal was removed, and the mixture allowed to vent for 2 h to remove excess CO_2. Aminated glycans **3** were lyophilized overnight, then placed under argon and dissolved in 5 mL anhydrous dimethyl

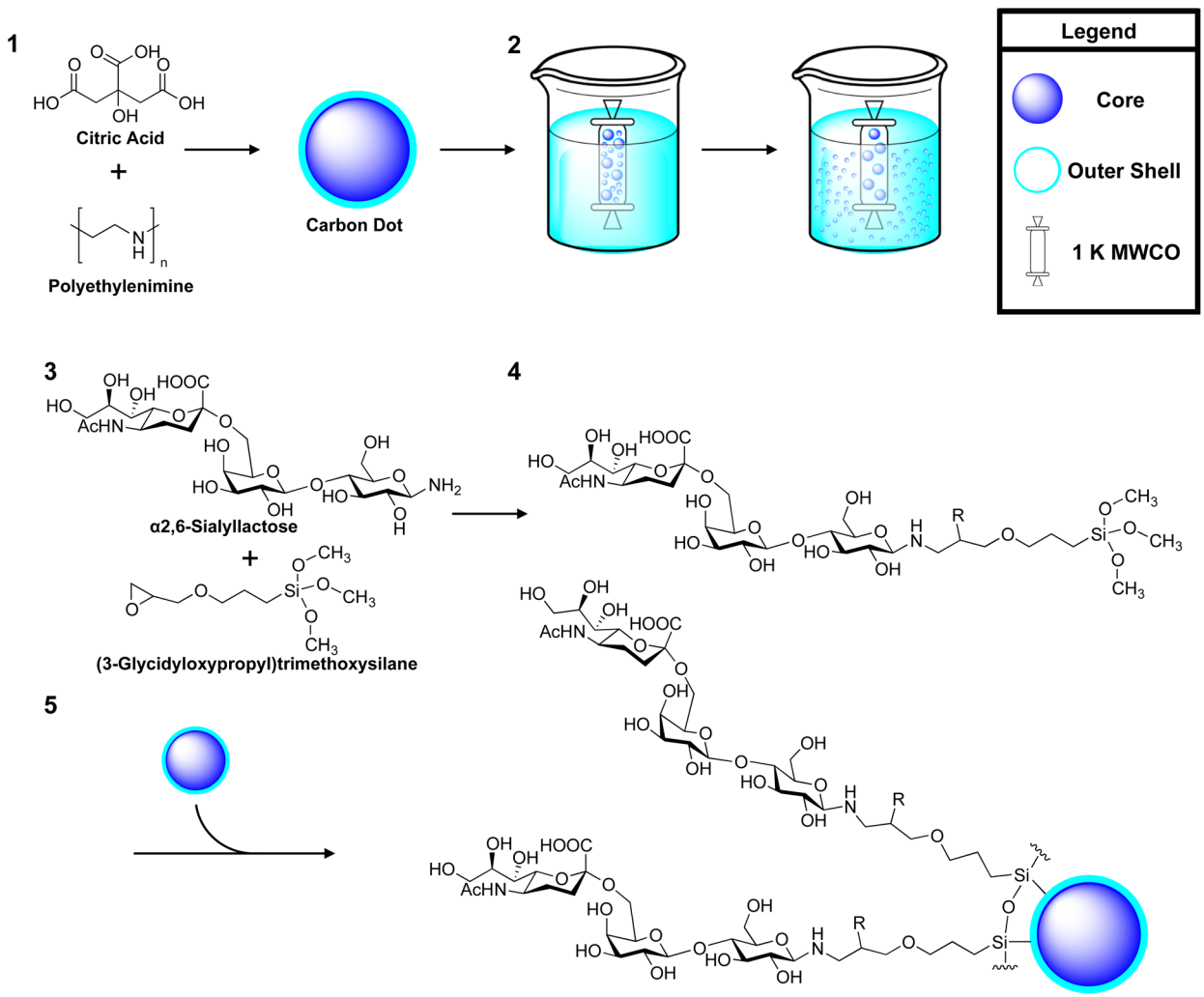

Scheme 1 An overview of the synthesis of α2,6-sialyllactose (2,6-SL) coated carbon dots (CD). Synthesis reagents and conditions, 1 citric acid and polyethyleneimine (MW ~ 800) (1 : 20) in 5 mL distilled water, treated in a Teflon-lined autoclave at 180 °C for 6 h; 2 dialysis in distilled water against 1 K MWCO to remove larger particles, only the dialysate was kept; 3 amination of 2,6-SL. Ammonium carbonate (1 : 5 molar excess) in ammonium hydroxide, 50 °C, 3 days; 4 silanization of 2,6-SL with GOPTS. Anhydrous DMSO : DMF (1 : 1), GOPTS in anhydrous methanol, 40 °C, overnight, acetic anhydride, DMAP, 4 °C, 15 min; 5 passivation to uCD. Anhydrous methanol, RT, overnight. R group indicates position of acetyl moiety after acetylation.

sulfoxide (DMSO) and *N*,*N*-dimethylformamide (DMF) (v/v, 1 : 1). Anhydrous 3-(glycidyloxypropyl)trimethoxysilane (2%, v/v) was added to the mixture and allowed to react at 40 °C overnight to form either a lactose-GOPTS, 2,6-SL-GOPTS or 2,3-SL-GOPTS conjugate **4**. The epoxy-ring was acetylated to prevent ring opening. Here, the product was cooled to 4 °C and neutralized with acetic anhydride and 4-dimethylaminopyridine (DMAP) (1 : 1 : 2, molar equivalents) for 15 min and stopped with the addition of methanol (1 : 1, v/v). The mixture was allowed to warm to RT and 10 mg of uCD **5** (in anhydrous methanol) was added and allowed to react overnight. The resulting products were first dialysed against 3.5 K MWCO (Spectrum Inc.) in MilliQ water for 16 h to remove larger aggregates of glyco-CDs. The particles <3.5 kDA were subsequently lyophilized and dialysed against 1 K MWCO (Spectrum Inc.) in 1 L of water for 16 h. Here, the particles >1 kDA were retained and lyophilized overnight to be used as test compounds. As all glyco-coated CDs were produced through self-assembly around uCD, they are all share a similar core identity only differing by their coat. As such they will be referred to hereafter as; 6-CD for 2,6-SL coated uCD, 3-CD for 2,3-SL coated uCD and Lac-CD for lactose coated uCD.

Quantification of glycan conjugation to carbon dot. Detection and quantification of the respective glyco-coat of 6-CD, 3-CD and Lac-CD was performed using anthrone reagent as described.[51] In brief a stock solution of ACS (97%) anthrone (Sigma-Aldrich) was prepared by dissolving 20 mg of anthrone into 10 mL concentrated ACS (98%) sulphuric acid (Sigma-Aldrich) and protected from light. Lactose disaccharides were used as a standard to quantitate the carbohydrate concentration of each CD. In glass vials, 400 μL of anthrone reagent was added to 200 μL of each standard or test compound, heated in a boiling water bath for 15 min and cooled in an ice bath. 200 μL of each sample was aliquoted into a 96 well plate and absorbance measured at 622 nm using an Infinite M200 Pro Multimodal Plate reader (Tecan). A linear calibration curve ($y = 0.001x + 0.0386$, $R2 = 0.9969$) was obtained by plotting absorbance against concentration of lactose on Microsoft EXCEL. The extent of the CD glyco-coat functionalization was determined using the above calibration curve. The molar concentration was calculated based on the respective concentrations of glycans in each carbon dot sample and subsequently used to compare monovalent glycan concentrations to multivalent glyco-coated carbon dot concentrations.

Biological verification and investigations

Hapten inhibition assays. Throughout this study recombinant Fc-chimeras were used. They compromised of the N-terminal three Ig-domains of the respective siglecs fused C-terminally to the Fc-part of human IgG1. Expression of siglec-1 and CD22 in Cho Lec1 cells as well as protein purification were performed as described.[52,53] Fetuin-containing α(2,3)- and α(2,6)- linked Sia was used as a target in hapten inhibition assays since both siglecs studied here bind to this glycoprotein. These assays were performed as described[54] using black, high binding 384, microplates (OptiPlate, PerkinElmer) to determine the half maximal inhibitory concentration of siglec binding (IC_{50}) to monovalent 2,3-SL and 2,6-SL and multivalent 6-CD, 3-CD and Lac-CD. Briefly, siglec Fc-chimeras and anti-hu-IgG-AP were allowed to bind to immobilized fetuin for 4 h at 4 °C. Subsequent binding curves of fluorescein diphosphate cleavage by alkaline phosphatase were used to attain maximum binding of siglec. To test for inhibition, glyco-coated CDs were incorporated into the siglec Fc-chimeras and anti-hu-IgG-AP cocktail at various concentrations as competitive inhibitors against immobilized fetuin. Specific binding was obtained by subtracting the average of non-specific binding of probes to immobilized asialofetuin. IC_{50} was determined from corresponding binding curves. For a better comparison between different assays, for each sample its relative IC_{50} (rIC_{50}) was calculated from its IC_{50} ($IC_{50Sample}$) and the IC_{50} of the monovalent 2,3-SL or 2,6-SL; (IC_{50Ref}): $rIC_{50} = IC_{50Ref}/IC_{50Sample}$. Each sample was measured in triplicates and each experiment was repeated at least three times. Finally, average rIC_{50} values and corresponding standard deviations were calculated from these experiments. Standard deviations for all compounds were below 15% of the average rIC50 values.

Cell viability assays. BL Daudi cells with confirmed CD22 expression (see flow cytometry methods) were treated with uCD, Lac-CD and 6-CD to compare the cytotoxic effects of each CD. As CDs are naturally fluorescent, the luminescent RealTime-Glo™ MT Cell Viability Assay (Promega) was performed as per manufacturer's instructions. In brief, cells were counted using a Neubauer haemocytometer (Marienfeld) and 1×10^4 cells per well were seeded into a white opaque 96 well plate (CulturPlate-96, PerkinElmer). For end point assays, the RealTime Glo reagent was mixed with CDs at varying concentrations and allowed to incubate overnight. Luminescence was measured at an integration of 1 s at 37 °C using an Infinite® 200 Pro (Tecan). Real time monitoring of cell viability was performed using this same instrument with interval reads every 20 min over the course of 20 h. Finally, to compare multivalent and monovalent interactions, MT cell viability assays were performed with 6-CD at 1 mg mL^{-1} in the presence of 2,6-SL. Here, BL Daudi cells were incubated for 24 h before performing luminometry measurements using the Infinite® 200 Pro.

Flow cytometry. BL Daudi suspension cells were tested for CD22 expression using an anti-CD22 antibody [RFB4] with phycoerythrin (Ex: 488 nm, Em: 575 nm) (abcam). Flow cytometry was performed as described manufactures instructions. After confirmation of CD22+ expression BL Daudi were counted using a Neubauer haemocytometer (Marienfeld). Cells were washed with PBS and resuspended (5×10^6 cells per mL) in phosphate buffer (pH 7.4) containing freshly dissolved 2 mM $NaIO_4$ and incubated for 30 min at 4 °C in the dark. Excess periodate was destroyed by adding 10 μL of 20% glycerol. 5×10^4 cells per mL were seeded into falcon tubes. Blocking buffer was prepared fresh, by dissolving 1% BSA in PBS (w/v). Washing buffer was prepared fresh by dissolving 0.1% BSA (w/v) in PBS. Cell were blocked with blocking buffer for 1 h at 4 °C and then washed three times in washing buffer. Cells were incubated with either 100 μg uCD, Lac-CD or 6-CD for 30 min at 4 °C, followed by three more washes. Competitive binding assays

with 100 μg of 6-CD in the presence of 10 μg of methyl-α-9-*N*-(biphenyl-4-carbonyl)-amino-9-deoxy-Neu5Ac (BPC-Neu5Ac)[53] was performed on both periodate treated and untreated BL Daudi cells in the same manner described above. Flow cytometry was performed using a CyAn ADP (Beckman Coulter) with a 405 nm excitation laser and a 450/50 nm emission filter.

Results

Assembly and characterization of sialoglyco-CDs

In this study, four different CDs were employed to probe the interaction of multivalently displayed Sia with siglec. Here, SAGMs of lactose, α(2,6)-sialyllactose (2,6-SL) and α(2,3)-sialyllactose (2,3-SL) were generated using the epoxide functionality of GOPTS and employed to decorate CDs, thus imparting glycan functionality. Within this study, uncoated CD (uCD) and lactose-CD (Lac-CD) have both previously been extensively characterized, providing proof-of-principle for our synthesis as illustrated in Scheme 1.[47,55] Subsequent generation of 6-CD and 3-CD was achieved through passivation to uCD with either a 2,6-SL or 2,3-SL SAGM, respectively. Here, amination of the anomeric carbonyl of glucose in 2,6-SL and 2,3-SL is performed to ensure the Sia moiety faces away from the CD core. Due to the higher reactivity of the amine group at the reducing end of glucose, the epoxy ring present in GOPTS affords us control in positioning the direction of the glycan ligands. The synthesis and conjugation of the glycan-silylate intermediate and SAGM passivation to uCD are outlined in Scheme 1. Importantly, self-assembly of the glycan monolayer occurs on the surface of the CD as the silanol hydrogen is far more electrophilic and therefore reactive when compared to the hydrogen of the carbinol moiety. Due to this difference in the electropositive silicon, a higher dipole moment for the silanol group occurs leading to greater hydrogen bonding to the CD.

We have previously shown, that passivation of the glycan-silylate intermediates of SAGM on the CDs leads to a broader blue shift of the PL peak compared to uCD.[47] This phenomenon was also observed for 6-CD and 3-CD with similar excitation peaks at 360 nm, indicating successful modification of uCD surface functional groups (see ESI, Fig. S2†). Of note, 3-CD also exhibited additional features, with lines of emission across several frequencies (415 and 430 nm) corresponding to excitation of 380 nm. This bimodal excitation has been similarly observed in uCD indicating there was still unreacted uCD present in this sample. Fourier transform infrared spectroscopy (FTIR) of both 3-CD and 6-CD (see ESI, Fig. S3†) confirmed the generation of the silicon network that forms the backbone of the SAGM. Here a sharp band at 980 cm^{-1} be ascribed to the Si–O–Si network. The small sharp peak positioned at 1100 cm^{-1} is likely due to the Si–C bond, and the large absorption band cantered at 875 cm^{-1} from the Si–N bond to PEI. Finally, we acquired the TEM for 6-CD and 3-CD (see ESI, Fig. S4†), which clearly shows a well-defined carbon core with a reduced area of density surrounding the core. DLS analysis (see ESI, Table S1†) illustrated a monodisperse population with size ranging from 70–90 nm, which is consistent with our previous findings.

To unambiguously confirm that uCD was decorated with our Sia-SAGMs, we employed ^{1}H NMR spectroscopy. Consistent with our previous findings,[47] the ring and anomeric protons of both 2,6-SL and 2,3-SL SAGM remain chemically unchanged through passivation to the uCD surface. ^{1}H NMR spectra of 6-CD and 3-CD (see ESI Fig. S5 and S6†) revealed that the anomeric proton of the glucose moiety (GlcH-1) is predominantly covalently linked in the α-anomeric configuration to the GOPTS linker. Interestingly, this preference was absent in our previously characterized Lac-CD.[47] To confirm that 2,6-SL and 2,3-SL glycans were conjugated correctly on 6-CD and 3-CD, we monitored the H3 equatorial and axial protons (H3eq/H3ax) of the Sia moiety as displayed in each panel of the ^{1}H NMR spectra. The H3ax proton for 3-CD (∼1.82 ppm) and 6-CD (∼1.76 ppm) revealed that both CDs are uniquely distinct due to their glycosidic linkage. This is further supported by the H3eq protons of 3-CD (∼2.78 ppm) that appear as a pronounced doublet of doublet appearing upfield of the H3eq protons on 6-CD (∼2.75 ppm). The presence of protons resonating from the Sia moiety not only confirms successful passivation but more importantly, also pre-organisation and complete solvent exposure of the Sia residue.

The calculation of the molar concentration of glycosylated CDs was performed using the anthrone assay.[56] Here, the molar concentration was revealed to be 356 ± 42.57 μM for Lac-CD, 382 ± 49.12 μM for 6-CD and 290 ± 55.56 μM for 3-CD. These values allowed direct comparison of concentrations used with monovalent glycans in subsequent experiments. Of note, the decreased molar concentration of 2,3-SL compared to Lac-CD and 6-CD supports the findings from the PL spectra of 3-CD which detected unreacted uCD. Using the already calculated molarity of the glycan coated CDs from the anthrone assay, the number of molecules per carbon dot can be derived from the below eqn (1):

$$\frac{\left(\frac{g}{\mathrm{MW}}\right) \times N_{\mathrm{A}}}{n} \quad (1)$$

where, g is the grams of glycan calculated from the molarity quantified using the anthrone assay, MW is the molecular weight of the glycan, N_{A} is Avogadro's number and n is the number of CDs per litre. The number of CDs per litre can be calculated using the below equation:

$$n = \frac{w}{p \times d} \quad (2)$$

where, w is the weight concentration of CD (kg L^{-1}), p is the individual particle weight and d is the nanocarbon density assumed to be 1800 kg m^{-3} (based on the density of graphite). Using these two equations the number of glycan moieties on each CD was calculated to be 13 ± 2 copies for Lac-CD, 14 ± 2 for 6-CD and 11 ± 2 copies for 3-CD. Based on our findings, our permissible characterisation of 3-CD and 6-CD indicates that these multivalent sialosides can act as appropriate probes for siglec analyses.

Hapten inhibition assays

In order to determine the relative inhibitory potential of 3-CD and 6-CD compared to their monovalent counterparts (2,3-SL

Table 1 Comparison of inhibitory potential of CD-sialosides. Hapten inhibition assays revealed IC_{50} values of tested compounds using least three titrations, standard deviations were within 15%

	Siglec-1		CD22	
Compound	IC_{50} (μM)	rIC_{50}[a]	IC_{50} (μM)	rIC_{50}[b]
2,3-SL	232.3	1	n.i[c]	n.i[c]
2,6-SL	584.7	0.4	156.1	1
6-CD	135.0	1.7	67.9	2.3
3-CD	15.4	15.1	n.ic	n.ic
Lac-CD	n.i[c]	n.i[c]	n.i[c]	n.i[c]

[a] rIC_{50} values were calculated against 2,3-SL (IC_{50} 232.3 μM) as a reference compound. [b] rIC_{50} values were calculated against 2,6-SL (IC_{50} 156.1 μM) as a reference compound. [c] Not inhibitory against 1.5 mM. Individual IC_{50} curves are presented in the ESI Fig. S7.

and 2,6-SL), hapten inhibition assays with CD22 and siglec-1 were performed using immobilized fetuin as the Sia donor. Here, the equivalent micromolar concentrations of glycosylated-CDs, as calculated from the anthrone assay, were used to determine IC_{50} values for siglec-1 and CD22. Table 1 confirms similar inhibition of siglec activity as previously reported for 2,3-SL and 2,6SL,[7,57–60] and Lac-CD (the "asialylated" control) was unable to inhibit either siglec-1 or CD22. As expected, 3-CD and 6-CD showed significant increases in inhibition against their respective siglec targets compared to their monovalent equivalent. For siglec-1, a 15-fold increase in inhibition was observed for 3-CD compared to monovalent 2,3-SL. Additionally, although 2,6-SL is not the preferred substrate for siglec-1, when displayed multivalently, as is the case with 6-CD, a 1.7-fold increase in rIC_{50} compared to monovalent 2,3-SL was also observed. This indicates that Sia linkage-specific binding to siglec-1 can be partially overcome by increasing the multivalency of Sia ligands. Moreover 6-CD displayed a 4.3-fold increase in rIC_{50} compared to its monovalent 2,6-SL parent compound against siglec-1. For CD22, as expected 3-CD was not shown to be inhibitory, while 6-CD demonstrated a 2.3-fold increase in rIC_{50} compared to 2,6-SL. Of note, the IC_{50} of 6-CD (67.9 μM) is comparable to that of the known CD22 sialoside inhibitor, methyl-α-9-*N*-(biphenyl-4-carbonyl)-amino-9-deoxy-Neu5Ac (BPC-Neu5Ac:IC_{50}:35 μM).[61] Taken together, this suggests that the multivalent display of Sia significantly increases avidity of simple glycans.

BL daudi cell viability assays

To further explore the effect that the presentation of Sia moieties and multivalency has on siglec binding in more detail, we investigated the toxicity of our CDs on Burkitt's Lymphoma (BL) Daudi cells. Real time luminometry measurements (20 min intervals) was performed with cell viability being monitored for 20 h to provide a detailed examination of cell growth (Fig. 2). Interestingly, after 4 h of uCD treatment (Fig. 2, yellow), BL Daudi cells revealed a 2-fold increase in cell viability as measured through mitochondrial reductase activity. Compared to our control, which clearly do not divide as rapidly, these findings suggest that uCD may induce mitochondrial

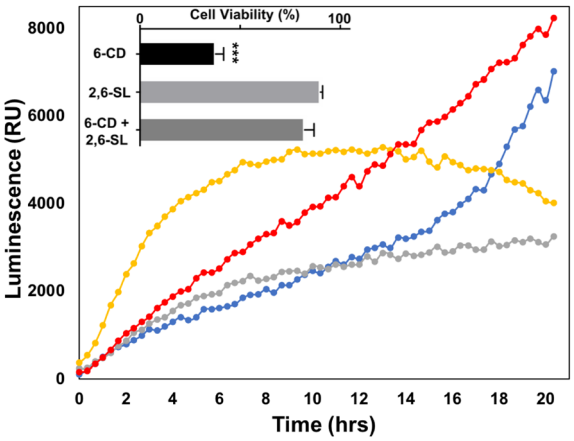

Fig. 2 Realtime cell viability of BL Daudi cells with various carbon dots, 6-CD (grey); uCD (yellow); Lac-CD (blue). The bar graph insert is a 24 h endpoint reading of multivalent 6-CD, monovalent 2,6-SL and a mixture of 6-CD and 2,6-SL. RPMI control is indicated by *.

hyperactivation leading to increase metabolic viability and MTT reduction. This is apparent after 14 h, where the BL Daudi cell population suddenly declines. We have previously reported that following lysosomal escape, uCD is capable of co-localization within the mitochondria of HeLa cells.[47] A similar mechanism may occur in BL Daudi cells, with uCD targeting the mitochondria leading to hyperactivation and increased MTT reduction. On the other hand, 6-CD (Fig. 2, grey) and Lac-CD (Fig. 2, blue) maintain comparable, albeit reduced metabolic activity, compared to the control (Fig. 2, red) up to 14 h. Beyond this point, however Lac-CD cytotoxicity is eventually overcome by the BL Daudi cells. This phenomenon was not apparent for 6-CD indicating that the Sia moiety is a strong determinant for sustained BL Daudi cytotoxicity. This was confirmed by the addition of 10 mM 2,6-SL, which abolished cell death (see bar graph insert in Fig. 2).

Flow cytometric analysis of CDs

Flow cytometric analysis was performed to assess the extent to which 6-CD, Lac-CD and uCD can be recognized by surface receptors present on BL Daudi cells. CD22+ expression (Fig. 3A) on BL Daudi cells was confirmed before exploring whether cytotoxicity of 6-CD in BL Daudi cells is driven through interaction with CD22. Here, mild periodate treatment was performed to truncate endogenous linked Sia leading to unmasking of CD22.[10] Initial probing of the Daudi cells with uCD and Lac-CD revealed contrasting interactions. Fig. 3B reveals an 8.5-fold increase in fluorescence for uCD compared to the control, likely due to the cationic nature of uCD leading to increased electrostatic interaction with the cell membrane and subsequent endocytosis.[62] This is supported by the finding that Lac-CD exhibited only a 1.3-fold increase in fluorescence compared to the control, suggesting that the presence of the Lac coat is decreasing the non-specific electrostatic interaction associated with uCD. Fig. 3C demonstrates specific interaction of 6-CD with CD22, with an 8-fold increase in binding observed

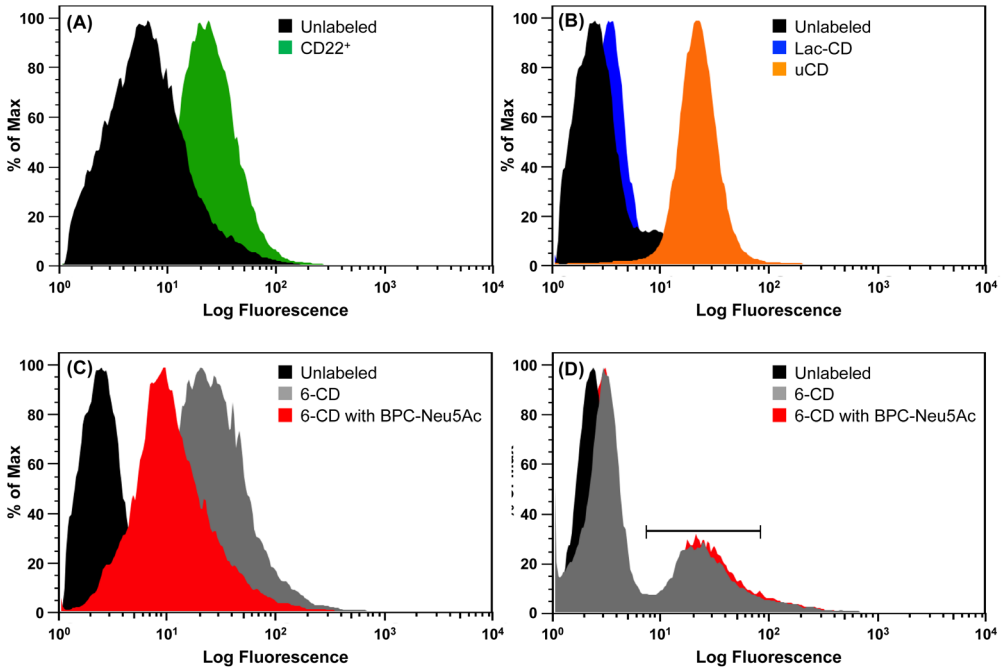

Fig. 3 Flow cytometric analysis of various CDs interacting with CD22+ Daudi cells. (A) Unlabeled (black), median: 9.87; anti-CD22 antibody (green), median: 29.8. (B) Unlabeled (black), median: 2.65; 100 μg Lac-CD (blue), median: 3.6; 100 μg uCD (orange), median: 22.6. (C) Unlabeled (black), median: 2.65; 100 μg 6-CD (grey), median: 21.6; 100 μg 6-CD with 10 μg BPC-Neu5Ac (red), median: 10.3. (D) B cells were not pretreated with periodate. Unlabeled (black), median: 2.31; 100 μg 6-CD (grey), median 3.67, scale bar represents 30% of Daudi population, median; 23.7; 100 μg 6-CD with 10 μg BPC-Neu5Ac (red), median: 3.84, scale bar represents 35% of Daudi population, median; 27.

to the unlabelled Daudi population. Importantly, 6-CD bound with 6-fold higher affinity to BL Daudi cells compared to Lac-CD, highlighting that the α(2,6)-linked Sia linkage is the major determinant for binding of these CDs. Additionally, binding of 6-CD to BL Daudi cells could be inhibited by BPC-Neu5Ac, a known potent inhibitor of CD22,[61] therefore unambiguously confirming 6-CD interaction with CD22. Our data clearly shows that the multivalent display of α(2,6)-linked Sia on CDs achieved using our SAGM approach permits specific targeting of CD22 on B cells.

Given the specific interaction of 6-CD to BL Daudi cell, we sought to further explore whether multivalent siglec ligands could be used to probe masked (non-periodate treated) BL Daudi cells. Fig. 3D shows that 6-CD possessed high enough avidity to compete with the *cis* ligands that normally mask CD22 on BL Daudi cells. Here, only a small population of BL Daudi cells (~30%) demonstrated a 10-fold increase in interaction with 6-CD. This indicates that masked CD22 is still capable of dampening the affinity of 6-CD to the entire BL Daudi population. Importantly, this interaction could not be inhibited by monovalent BPC-Neu5Ac, that has a 2-fold better IC_{50} compared to 2,6-linked sialosides, suggesting that 6-CD is binding to CD22 only through *trans* interactions.

Discussion

The challenge to design targeted siglec sialosides has been explored in great detail,[63–69] however the use of sialosides on multivalent nanoparticles is limited.[28,70–72] Based on our findings, we demonstrate that CDs are suitable scaffolds for biologically relevant multivalent display of sialosides to target siglecs as well Sia-recognizing receptors. In light of the varied cellular responses seen across BL Daudi cells treated with CDs, our work highlights unique biological responses from exposure to multivalent glycan scaffolds. Additionally, further research into the effect that the CD itself has on cellular interactions would provide useful insight into how these architectures can be modified to promote targeted endocytosis and uptake. Herein, we have sought to provide the framework for further design of intelligent multivalent sialylated CDs that can be used as targeted drug delivery systems for BL Daudi cells.

Thanks to the inherent fluorescence of these next-generation sialosides we were able to explore through flow cytometric analysis that cytotoxicity of 6-CD in BL Daudi cells was driven through *trans* interactions with CD22 (see Fig. 3D). We propose, that 6-CD interaction with CD22 allows phosphorylation of ITIMS by the kinase Lyn and subsequent recruitment of SHP-1 to negatively regulate BCR signal. Studies have demonstrated that the concentration of α(2,6)-linked Sia present on the B cell surface is estimated to be in the region of 25–30 mM,[25,73] around 100-fold higher than the K_D of CD22 for α2,6-linked Sia (0.1–0.3 mM (ref. 74–76)). These findings indicate CD22 is capable of *cis* interaction with glycoprotein ligands on the same cell. Our hapten inhibition assays revealed only a 2-fold increase in affinity for 6-CD to CD22 compared to α2,6-linked Sia, therefore it is challenging to suggest that 6-CD is capable of *cis* interactions with CD22.

Flow cytometry experiments revealed that 'unmasking' of CD22 by mild periodate treatment and removal of active Sia moieties, enables strong 6-CD binding. Binding of 6-CD to CD22 was limited in non-periodate treated BL Daudi cells, suggesting that 6-CD interact with CD22 on the B-cell surface through *trans* interactions. Our work supports previous findings[77] that *cis* ligands downregulate but do not prohibit binding of ligands in *trans*. *In vivo*, B cells are known to exploit *trans* interactions to allow recirculating back to the bone marrow by binding to ligands that are expressed on sinusoidal endothelium.[78] Additionally, it has been shown that binding of higher affinity multivalent probes to CD22 (ref. 77) or redistribution of CD22 (ref. 75) does not require unmasking. These studies highlighted a dynamic equilibrium where CD22 can switch between *cis* and *trans* interactions, depending on their relative affinity/avidity.

Further, our 6-CD findings are consistent with work performed by Collins *et al.*, where it was concluded that *cis* ligands regulate siglec binding to biologically relevant *trans* ligands. This is achieved through thresholds set by *cis* ligands to control binding of CD22 by *trans* interactions.[25,79,80] Importantly, studies into subpopulations of B cells have shown that cells can exist in both an unmasked state and that CD22 unmasking can occur after B cell activation.[81,82] Taking this into consideration, as 6-CD binding to CD22 in masked BL Daudi cells could not be inhibited by the addition of BPC-Neu5Ac, this indicates that CD22 interacts with 6-CD in *trans* and this is favoured over the binding of ligands in *cis*.

Cross-linking studies have indicated that multivalency is important to achieve functional interactions with CD22.[74] In our study, the multivalent nature of sialoglyco-CDs permits binding of more than one copy of CD22 receptor molecules. This is compounded especially given that CD22 forms homo-oligomers in resting B cells which would greatly increase the avidity of CD22–ligand interactions.[83–85] A study by Gasparrini *et al.*, (2016)[86] using super-resolution imagining techniques demonstrated that CD22 is organised as nanoscale clusters in resting B cells. Transgenic mice expressing CD22 mutants showed that the Sia binding domain of CD22 has a major contribution in defining both lateral mobility and nanocluster organisation.[86] Given this nanoscale clustering of CD22, it is likely that initial *trans*-interactions promote further binding of adjacent 2,6-SL moieties on our multivalent 6-CD. This in line with previous observations that suggest that low affinity binding events might be important in order to ensure that CD22 association, and allow the signalling event to be rapidly reversible.[87] Further, as CD22 redistributes to the site of cell contact,[80] it follows that the avidity of this interaction would also be increased by this process. This is supported by the cell viability results (Fig. 2, bar graph insert) where monovalent 2,6-SL decreased the cytotoxic effects of 6-CD.

Conclusions

The significance of the interaction between Sia and siglecs in immune regulation, cancer and infectious disease is well documented, however its role in physiological and pathological processes remains poorly understood. Here, we report for the first time the use of our SAGM approach to generate sialoglyco-CDs as a scaffold for simple targeting of siglecs. Of note, hapten inhibition assays with 3-CD demonstrated an IC50 of 15 μM against siglec-1, equating to a 15-fold increase in affinity compared to 2,3-SL. Additionally, for 6-CD we show that the preference of α(2,3)-linked Sia for siglec-1 can be altered as a result of the multivalent display of Sia ligands present on the CD. Here, the high surface/volume ratios, and abundant surface functional groups of the CDs, provide a locally high glycan concentration that has a direct effect on linkage specificity. Finally, *trans* interactions of 6-CD with CD22 was confirmed as a driver of cytotoxicity in BL Daudi cells. Taken together, our work highlights the potential of glycoengineered CDs as novel fluorescent molecular probes for widespread applications in sialoglycoscience, pharmaceutical and medical applications. This versatile functional behaviour of sialoglyco-CDs generated using our simple SAGM approach provides non-invasive diagnostic imaging and therapeutic opportunities especially for drug delivery applications.

Author contributions

The manuscript was written through contributions of all authors. OC wrote the initial draft of the paper, performed all the experiments, data analysis and generated the figures. QL provided the carbon dots. TH and OC performed the NMR characterization. MW and SK devised the hapten inhibition assays which were performed by OC. JT and TH conceived, designed, coordinated and revised the paper. JT planned together with OC all experiments. All authors have given approval to the final version of the manuscript.

Conflicts of interest

There are no conflicts to declare.

Acknowledgements

TH and SK thank the Australia–Germany Joint Research Co-operation Scheme, Universities Australia for a research exchange programme. The authors thank Prof. Paul Crocker for the siglec-1 clone; Dr Judith Weber, Dr Andrea Maggioni and Mrs Stephanie Holt for expression of siglec-1; Prof. Mark von Itzstein, Dr Paul Madge and Dr Robin Thomson for supplying BPC-Neu5Ac; and James Scott for acquiring the photoluminescence spectra of 6-CD and 3-CD.

Notes and references

1 A. Varki and T. Angata, *Glycobiology*, 2006, **16**, 1R–27R.
2 P. R. Crocker, J. C. Paulson and A. Varki, *Nat. Rev. Immunol.*, 2007, **7**, 255–266.
3 S. Sato, A. S. Miller, M. Inaoki, C. B. Bock, P. J. Jansen, M. L. K. Tang and T. F. Tedder, *Immunity*, 1996, **5**, 551–562.
4 L. Nitschke, R. Carsetti, B. Ocker, G. Köhler and M. C. Lamers, *Curr. Biol.*, 1997, **7**, 133–143.

5 K. L. Otipoby, K. B. Andersson, K. E. Draves, S. J. Klaus, A. G. Farr, J. D. Kerner, R. M. Perlmutter, C. L. Law and E. A. Clark, *Nature*, 1996, **384**, 634–637.
6 T. L. O'Keefe, G. T. Williams, S. L. Davies and M. S. Neuberger, *Science*, 1996, **274**, 798–801.
7 S. Kelm, A. Pelz, R. Schauer, M. T. Filbin, S. Tang, M. E. de Bellard, R. L. Schnaar, J. A. Mahoney, A. Hartnell, P. Bradfield, *et al.*, *Curr. Biol.*, 1994, **4**, 965–972.
8 S. Kelm, R. Brossmer, R. Isecke, H. J. Gross, K. Strenge and R. Schauer, *Eur. J. Biochem.*, 1998, **255**, 663–672.
9 L. D. Powell and A. Varki, *J. Biol. Chem.*, 1994, **269**, 10628–10636.
10 N. Razi and A. Varki, *Proc. Natl. Acad. Sci. U. S. A.*, 1998, **95**, 7469–7474.
11 H. Floyd, L. Nitschke and P. R. Crocker, *Immunology*, 2000, **101**, 342–347.
12 N. Kawasaki, J. L. Vela, C. M. Nycholat, C. Rademacher, A. Khurana, N. van Rooijen, P. R. Crocker, M. Kronenberg and J. C. Paulson, *Proc. Natl. Acad. Sci. U. S. A.*, 2013, **110**, 7826–7831.
13 M. De Schryver, A. Leemans, I. Pintelon, D. Cappoen, L. Maes, G. Caljon, P. Cos and P. L. Delputte, *Immunobiology*, 2017, **222**, 797–806.
14 T. K. Bera, M. Onda, R. J. Kreitman and I. Pastan, *Leuk. Res.*, 2014, **38**, 1224–1229.
15 P. M. Chaudhary, S. Toraskar, R. Yadav, A. Hande, R.-A. Yellin and R. Kikkeri, *Chem.–Asian J.*, 2019, **14**, 1344–1355.
16 A. H. Courtney, E. B. Puffer, J. K. Pontrello, Z.-Q. Yang and L. L. Kiessling, *Proc. Natl. Acad. Sci. U. S. A.*, 2009, **106**, 2500–2505.
17 L. Nitschke, *Immunol. Rev.*, 2009, **230**, 128–143.
18 C. M. Nycholat, C. Rademacher, N. Kawasaki and J. C. Paulson, *J. Am. Chem. Soc.*, 2012, **134**, 15696–15699.
19 H. Prescher, A. Schweizer, E. Kuhfeldt, L. Nitschke and R. Brossmer, *ACS Chem. Biol.*, 2014, **9**, 1444–1450.
20 S. Mesch, K. Lemme, M. Wittwer, H. Koliwer-Brandl, O. Schwardt, S. Kelm and B. Ernst, *ChemMedChem*, 2012, **7**, 134–143.
21 P. D. Madge, A. Maggioni, M. Pascolutti, M. Amin, M. Waespy, B. Bellette, R. J. Thomson, S. Kelm, M. von Itzstein and T. Haselhorst, *Sci. Rep.*, 2016, **6**, 36012.
22 S. V. Shelke, G. P. Gao, S. Mesch, H. Gathje, S. Kelm, O. Schwardt and B. Ernst, *Bioorg. Med. Chem.*, 2007, **15**, 4951–4965.
23 C. D. Rillahan, E. Schwartz, R. McBride, V. V. Fokin and J. C. Paulson, *Angew. Chem., Int. Ed. Engl.*, 2012, **51**, 11014–11018.
24 C. D. Rillahan, E. Schwartz, C. Rademacher, R. McBride, J. Rangarajan, V. V. Fokin and J. C. Paulson, *ACS Chem. Biol.*, 2013, **8**, 1417–1422.
25 B. E. Collins, O. Blixt, S. Han, B. Duong, H. Li, J. K. Nathan, N. Bovin and J. C. Paulson, *J. Immunol.*, 2006, **177**, 2994–3003.
26 J. Paulson, *Nat. Preced.*, 2009, DOI: **10.1038/npre.2009.3549.1**.
27 S. Spence, M. K. Greene, F. Fay, E. Hams, S. P. Saunders, U. Hamid, M. Fitzgerald, J. Beck, B. K. Bains, P. Smyth, E. Themistou, D. M. Small, D. Schmid, C. M. O'Kane, D. C. Fitzgerald, S. M. Abdelghany, J. A. Johnston, P. G. Fallon, J. F. Burrows, D. F. McAuley, A. Kissenpfennig and C. J. Scott, *Sci. Transl. Med.*, 2015, **7**, 303ra140.
28 C. L. Schofield, M. J. Marin, M. Rejzek, P. R. Crocker, R. A. Field and D. A. Russell, *Analyst*, 2016, **141**, 5799–5809.
29 M. Ohmae, M. Kojima, K. Mihara, Y. Yamazaki, I. Hara, E. Hara and S. Kimura, *Bioorg. Med. Chem. Lett.*, 2016, **26**, 4976–4982.
30 R. Yadav, P. Madhukar Chaudhary, B. Subramani, S. Toraskar, H. Bavireddi, R. V. Murthy, S. Sangabathuni and R. Kikkeri, *ACS Appl. Mater. Interfaces*, 2018, **10**, 28322–28330.
31 H. Zhang, J. Zhao, X. Gu and Y. Wen, *J. Nanopart. Res.*, 2019, **21**, 154.
32 W. Peng and J. C. Paulson, *J. Am. Chem. Soc.*, 2017, **139**, 12450–12458.
33 M. K. O'Reilly and J. C. Paulson, *Trends Pharmacol. Sci.*, 2009, **30**, 240–248.
34 P. R. Crocker and P. Redelinghuys, *Biochem. Soc. Trans.*, 2008, **36**, 1467–1471.
35 W. C. Chen, G. C. Completo, D. S. Sigal, P. R. Crocker, A. Saven and J. C. Paulson, *Blood*, 2010, **115**, 4778–4786.
36 C. D. Rillahan, M. S. Macauley, E. Schwartz, Y. He, R. McBride, B. M. Arlian, J. Rangarajan, V. V. Fokin and J. C. Paulson, *Chem. Sci.*, 2014, **5**, 2398–2406.
37 W. C. Chen, D. S. Sigal, A. Saven and J. C. Paulson, *Leuk. Lymphoma*, 2012, **53**, 208–210.
38 L. Otten, D. Vlachou, S. J. Richards and M. I. Gibson, *Analyst*, 2016, **141**, 4305–4312.
39 D. Benito-Alifonso, S. Tremel, B. Hou, H. Lockyear, J. Mantell, D. J. Fermin, P. Verkade, M. Berry and M. C. Galan, *Angew. Chem., Int. Ed. Engl.*, 2014, **53**, 810–814.
40 M. D. Oliveira, C. A. Andrade, M. T. Correia, L. C. Coelho, P. R. Singh and X. Zeng, *J. Colloid Interface Sci.*, 2011, **362**, 194–201.
41 T. D. Farr, C. H. Lai, D. Grunstein, G. Orts-Gil, C. C. Wang, P. Boehm-Sturm, P. H. Seeberger and C. Harms, *Nano Lett.*, 2014, **14**, 2130–2134.
42 D. Benito-Alifonso, S. Tremel, B. Hou, H. Lockyear, J. Mantell, D. J. Fermin, P. Verkade, M. Berry and M. C. Galan, *Angew. Chem., Int. Ed. Engl.*, 2014, **53**, 810–814.
43 C. Dalal and N. R. Jana, *J. Phys. Chem. C*, 2018, **122**, 25651–25660.
44 E. Han, L. Ding, S. Jin and H. Ju, *Biosens. Bioelectron.*, 2011, **26**, 2500–2505.
45 Y. Guo, I. Nehlmeier, E. Poole, C. Sakonsinsiri, N. Hondow, A. Brown, Q. Li, S. Li, J. Whitworth, Z. Li, A. Yu, R. Brydson, W. B. Turnbull, S. Pohlmann and D. Zhou, *J. Am. Chem. Soc.*, 2017, **139**, 11833–11844.
46 S. A. Hill, D. Benito-Alifonso, D. J. Morgan, S. A. Davis, M. Berry and M. C. Galan, *Nanoscale*, 2016, **8**, 18630–18634.
47 O. Cooper, E. Eftekhari, J. Carter, B. Mallard, J. Kaur, M. J. Kiefel, T. Haselhorst, Q. Li and J. Tiralongo, *ACS Appl. Nano Mater.*, 2020, **3**, 7804–7817.

48 O. Cooper and J. Tiralongo, in *Comprehensive Glycoscience*, Elsevier, 2021, pp. 538–565, DOI: 10.1016/b978-0-12-819475-1.00012-2.
49 E. Eftekhari, W. Wang, X. Li, A. Nikhil, Z. Wu, R. Klein, I. S. Cole and Q. Li, *Sens. Actuators, B*, 2017, **240**, 204–211.
50 D. Vetter and M. A. Gallop, *Bioconjugate Chem.*, 1995, **6**, 316–318.
51 V. E. Turula Jr, T. Gore, S. Singh and R. G. Arumugham, *Anal. Chem.*, 2010, **82**, 1786–1792.
52 P. R. Crocker and S. Kelm, in *Weir's Handbook of Experimental Immunology*, ed. L. A. Herzenberg, D. M. Weir and C. Blackwell, Blackwell Science, Cambridge, 1996, pp. 166.1–166.11.
53 S. Kelm, P. Madge, T. Islam, R. Bennett, H. Koliwer-Brandl, M. Waespy, M. von Itzstein and T. Haselhorst, *Angew. Chem., Int. Ed.*, 2013, **52**, 3616–3620.
54 N. Bock and S. Kelm, *Methods Mol. Biol.*, 2006, **347**, 359–375.
55 E. Eftekhari, W. Wang, X. Li, A. Nikhil, Z. Wu, R. Klein, I. S. Cole and Q. Li, *Sens. Actuators, B*, 2017, **240**, 204–211.
56 V. E. Turula, T. Gore, S. Singh and R. G. Arumugham, *Anal. Chem.*, 2010, **82**, 1786–1792.
57 E. C. Brinkman-Van der Linden and A. Varki, *J. Biol. Chem.*, 2000, **275**, 8625–8632.
58 B. E. Collins, M. Kiso, A. Hasegawa, M. B. Tropak, J. C. Roder, P. R. Crocker and R. L. Schnaar, *J. Biol. Chem.*, 1997, **272**, 16889–16895.
59 K. Strenge, R. Schauer, N. Bovin, A. Hasegawa, H. Ishida, M. Kiso and S. Kelm, *Eur. J. Biochem.*, 1998, **258**, 677–685.
60 K. Hanasaki, L. D. Powell and A. Varki, *J. Biol. Chem.*, 1995, **270**, 7543–7550.
61 S. Kelm, J. Gerlach, R. Brossmer, C.-P. Danzer and L. Nitschke, *J. Exp. Med.*, 2002, **195**, 1207–1213.
62 E. Frohlich, *Int. J. Nanomed.*, 2012, **7**, 5577–5591.
63 C. M. Nycholat, C. Rademacher, N. Kawasaki and J. C. Paulson, *J. Am. Chem. Soc.*, 2012, **134**, 15696–15699.
64 H. Prescher, A. Schweizer, E. Kuhfeldt, L. Nitschke and R. Brossmer, *ACS Chem. Biol.*, 2014, **9**, 1444–1450.
65 S. Mesch, K. Lemme, M. Wittwer, H. Koliwer-Brandl, O. Schwardt, S. Kelm and B. Ernst, *ChemMedChem*, 2012, **7**, 134–143.
66 P. D. Madge, A. Maggioni, M. Pascolutti, M. Amin, M. Waespy, B. Bellette, R. J. Thomson, S. Kelm, M. von Itzstein and T. Haselhorst, *Sci. Rep.*, 2016, **6**, 36012.
67 S. V. Shelke, G. P. Gao, S. Mesch, H. Gathje, S. Kelm, O. Schwardt and B. Ernst, *Bioorg. Med. Chem.*, 2007, **15**, 4951–4965.
68 C. D. Rillahan, E. Schwartz, R. McBride, V. V. Fokin and J. C. Paulson, *Angew. Chem., Int. Ed. Engl.*, 2012, **51**, 11014–11018.
69 C. D. Rillahan, E. Schwartz, C. Rademacher, R. McBride, J. Rangarajan, V. V. Fokin and J. C. Paulson, *ACS Chem. Biol.*, 2013, **8**, 1417–1422.
70 S. Spence, M. K. Greene, F. Fay, E. Hams, S. P. Saunders, U. Hamid, M. Fitzgerald, J. Beck, B. K. Bains, P. Smyth, E. Themistou, D. M. Small, D. Schmid, C. M. O'Kane, D. C. Fitzgerald, S. M. Abdelghany, J. A. Johnston, P. G. Fallon, J. F. Burrows, D. F. McAuley, A. Kissenpfennig and C. J. Scott, *Sci. Transl. Med.*, 2015, **7**, 303ra140.
71 M. Ohmae, M. Kojima, K. Mihara, Y. Yamazaki, I. Hara, E. Hara and S. Kimura, *Bioorg. Med. Chem. Lett.*, 2016, **26**, 4976–4982.
72 R. Yadav, P. Madhukar Chaudhary, B. Subramani, S. Toraskar, H. Bavireddi, R. V. Murthy, S. Sangabathuni and R. Kikkeri, *ACS Appl. Mater. Interfaces*, 2018, **10**, 28322–28330.
73 B. E. Collins, O. Blixt, A. R. DeSieno, N. Bovin, J. D. Marth and J. C. Paulson, *Proc. Natl. Acad. Sci. U. S. A.*, 2004, **101**, 6104–6109.
74 L. D. Powell, R. K. Jain, K. L. Matta, S. Sabesan and A. Varki, *J. Biol. Chem.*, 1995, **270**, 7523–7532.
75 T. R. Bakker, C. Piperi, E. A. Davies and P. A. Merwe, *Eur. J. Immunol.*, 2002, **32**, 1924–1932.
76 Y. Suzuki, T. Ito, T. Suzuki, R. E. Holland Jr, T. M. Chambers, M. Kiso, H. Ishida and Y. Kawaoka, *J. Virol.*, 2000, **74**, 11825–11831.
77 O. Blixt and J. C. Paulson, *Adv. Synth. Catal.*, 2003, **345**, 687–690.
78 L. Nitschke, H. Floyd, D. J. Ferguson and P. R. Crocker, *J. Exp. Med.*, 1999, **189**, 1513–1518.
79 B. E. Collins, O. Blixt, N. V. Bovin, C. P. Danzer, D. Chui, J. D. Marth, L. Nitschke and J. C. Paulson, *Glycobiology*, 2002, **12**, 563–571.
80 B. E. Collins, O. Blixt, A. R. DeSieno, N. Bovin, J. D. Marth and J. C. Paulson, *Proc. Natl. Acad. Sci. U. S. A.*, 2004, **101**, 6104–6109.
81 N. Razi and A. Varki, *Glycobiology*, 1999, **9**, 1225–1234.
82 C. P. Danzer, B. E. Collins, O. Blixt, J. C. Paulson and L. Nitschke, *Int. Immunol.*, 2003, **15**, 1137–1147.
83 S. Han, B. E. Collins, P. Bengtson and J. C. Paulson, *Nat. Chem. Biol.*, 2005, **1**, 93–97.
84 C. L. Law, A. Aruffo, K. A. Chandran, R. T. Doty and E. A. Clark, *J. Immunol.*, 1995, **155**, 3368–3376.
85 S. Han, B. E. Collins, P. Bengtson and J. C. Paulson, *Nat. Chem. Biol.*, 2005, **1**, 93–97.
86 F. Gasparrini, C. Feest, A. Bruckbauer, P. K. Mattila, J. Muller, L. Nitschke, D. Bray and F. D. Batista, *EMBO J.*, 2016, **35**, 258–280.
87 T. F. Tedder, J. Tuscano, S. Sato and J. H. Kehrl, *Annu. Rev. Immunol.*, 1997, **15**, 481–504.